Radical Diffusion Crossover Phenomenon in Glass-Forming Liquids

Jakov Slade[†], Dalibor Merunka,*[,†] and Miroslav Peric[‡]

[†]Division of Physical Chemistry, Ruđer Bošković Institute, Bijenička cesta 54, HR-10000 Zagreb, Croatia

[‡]Department of Physics and Astronomy, California State University, Northridge, Northridge, California 91330, United States

March 10, 2022

*Corresponding author. E-mail: merunka@irb.hr, Tel: +3851-4561-136

Abstract

We studied the diffusivities of a nitroxide radical at various temperatures in six glass-forming molecular liquids by electron spin resonance. By comparing the radical diffusivities and solvent self-diffusivities, we found that the radical diffusivities are lower than the self-diffusivities at high temperatures and approach them at low temperatures in all liquids. This crossover behavior was considered as evidence that a single-molecule diffusion process transforms into a collective process with temperature lowering. The crossover phenomenon was analyzed by a novel, simple diffusion model, combining collective and single-molecule diffusion processes, and it was compared to the Arrhenius crossover phenomenon. The obtained results suggest that future studies of tracer diffusion could contribute to a better understanding of diffusion mechanisms in glass-forming liquids. The proposed diffusion model could be used to study the crossover phenomena of tracer diffusion measured by other techniques, and it could serve as a base for developing more advanced models.

TOC graphics

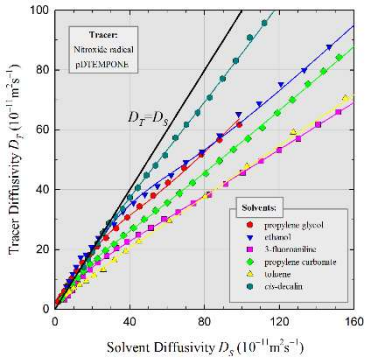

Keywords tracer diffusivity, self-diffusivity, glass transition, electron spin resonance, nitroxide radicals, molecular liquids

Translational diffusion of host molecules (self-diffusion) and diluted guest molecules (tracer diffusion) in molecular liquids have been studied by a number of experimental and theoretical methods because theoretical and practical interests.[1-3] If the guest molecule is a free radical, its diffusion can be studied by electron spin resonance (ESR). Because the relative motion of the radical's molecules modulates spin interactions between them, the shape of the ESR spectrum of the radical depends on its diffusion coefficient (diffusivity). By measuring the shape changes of the ESR spectrum with radical concentration, we obtain information about the radical diffusivity.[4-7]

Diffusion in glass-forming liquids shows interesting phenomena whose explanation could help to understand the nature of glass transition. One phenomenon, which is detected in many tracer and self-diffusivity measurements in the supercooled state (below the melting temperature T_m), is a great enhancement of diffusivity over that predicted by the Stokes-Einstein (SE) law.[8-11] The violation of the SE law appears below the crossover temperature $T_c \approx 1.2T_g$ (T_g is the glass transition temperature), and it strongly decreases as the tracer molecule exceeds the host molecule's size. This size effect supports the widely accepted view that the SE violation is associated with spatially correlated and heterogeneous dynamics in the supercooled state, but a clear connection between these two phenomena is yet to be established.[8-11]

Another phenomenon detected in diffusivity measurements in glass-forming metallic liquids is the Arrhenius crossover phenomenon at the temperature T_A, which is much higher than T_c.[12] This phenomenon denotes a change in the temperature dependence of diffusivity from the Arrhenius dependence above T_A into a stronger non-Arrhenius one below T_A. The Arrhenius crossover phenomenon is believed to reflect the onset of cooperativity in the motion of particles, which move relatively

independently above T_A and begin to move in a more correlated and cooperative fashion below T_A.[9-13] The relative crossover temperature in metallic liquids $\theta_A = T_A / T_g \approx 2$ was compared to θ_A in molecular and network liquids,[12] which were estimated from relaxation time and viscosity measurements.[13] It was found that θ_A is lower for more fragile glass formers, that is., those with the steeper temperature dependence of transport properties at T_g.[12] As the most fragile group of glass formers, molecular liquids exhibit $\theta_A \approx 1.4$, which means that T_A is close to T_m.

Several molecular dynamics simulations confirmed the belief that diffusive motion in a supercooled liquid becomes more cooperative and collective by the temperature decrease.[14-16] One of the scarce experimental pieces of evidence for this belief is a slight difference between the diffusivities of two isotopes of tracer atoms in a supercooled metallic liquid.[17] This very weak isotope effect was explained by the participation of several atoms in the diffusion process. It was argued that in this case, the rate of diffusion processes depends on the average mass of participating atoms, which diminishes the effect of the mass change of one participating atom. Unfortunately, there are not many experimental observations of cooperative diffusion below T_A. Therefore, more experimental evidence of cooperative diffusion motion would be desirable.

In this Letter, we report ESR results for the temperature dependences of the tracer diffusivity of a nitroxide radical $D_T(T)$ in six molecular glass formers. Following indications for coupling between diffusive motion of tracer and host molecules,[7] we determined the temperature dependences of self-diffusivity $D_S(T)$ in all liquids from the literature data (Figure S1 and Table S1 in SI1). It was revealed that $D_T(T)$ is lower than $D_S(T)$ at high temperatures and approaches $D_S(T)$ at low temperatures. We

considered the crossover behavior of $D_T(T)$ as evidence that diffusive motion in liquids becomes more collective upon cooling, and we analyzed this phenomenon using a simple diffusion model.

We studied the diffusivity of nitroxide radical pDTEMPONE (perdeuterated 2,2,6,6-tetramethyl-4-oxopiperidine-1-oxyl) in glass-forming liquids: propylene glycol (PG), ethanol (EtOH), 3-fluoroaniline (3-FA), propylene carbonate (PC), toluene (Tol), and *cis*-decalin (*c*-Dec). The chemical structures of the radical and solvents are presented in Figure S2 in SI2. In order to improve the method, we studied radicals labeled with ^{15}N and ^{14}N isotopes (^{15}N- and ^{14}N-pDTEMPONE), which have different ESR spectra but practically equal diffusivities.

Here, we give a brief overview of the ESR method for measuring radical diffusivity, which is described in more detail in SI3 and refs 7,18-19. First, we estimated the purities of pDTEMPONE radicals by using solutions of Fremy's salt radicals as standards.[20] Then, we recorded ESR spectra of 12 solutions with different concentrations of ^{15}N- and ^{14}N-pDTEMPONE in each solvent at various temperatures. We fitted all ESR spectra (Figure S3 and Table S2) to the theoretical ESR spectral function for solutions of ^{15}N- and ^{14}N-labeled radicals with spin interactions.[5,7,18,19] The best-fit values of the spin coherence-transfer rate Λ, which is the best ESR parameter to study radical diffusion, were fitted to a linear function of radical concentration at each temperature (Figure S4). The linear concentration coefficient of Λ, determined as the slope of the linear function, was compared to its theoretical dependence on radical diffusivity (Figure S5). In theoretical treatment, we modeled dissolved radicals as continuously diffusing hard spheres and applied formalism of the kinetic equations for the spin density matrices of radicals.[4,7,18,19,21] From this comparison, we obtained the diffusivities of ^{15}N- and ^{14}N-pDTEMPONE at each temperature, which show similar values (Figure 1). The diffusivity of pDTEMPONE, calculated as

the average value of the diffusivities of ^{15}N- and ^{14}N-pDTEMPONE, is presented as a function of temperature in all liquids (Figure 1).

Figure 1. (a) Diffusivities versus temperature for ^{15}N- and ^{14}N-pDTEMPONE radicals in PC. (b,c,d) Diffusivities of pDTEMPONE (empty symbols) and fitted self-diffusivities (filled symbols) versus temperature in studied liquids. The full and dashed lines denote the radical diffusivity fits to eq 3 and their extrapolated high-temperature dependences, respectively.

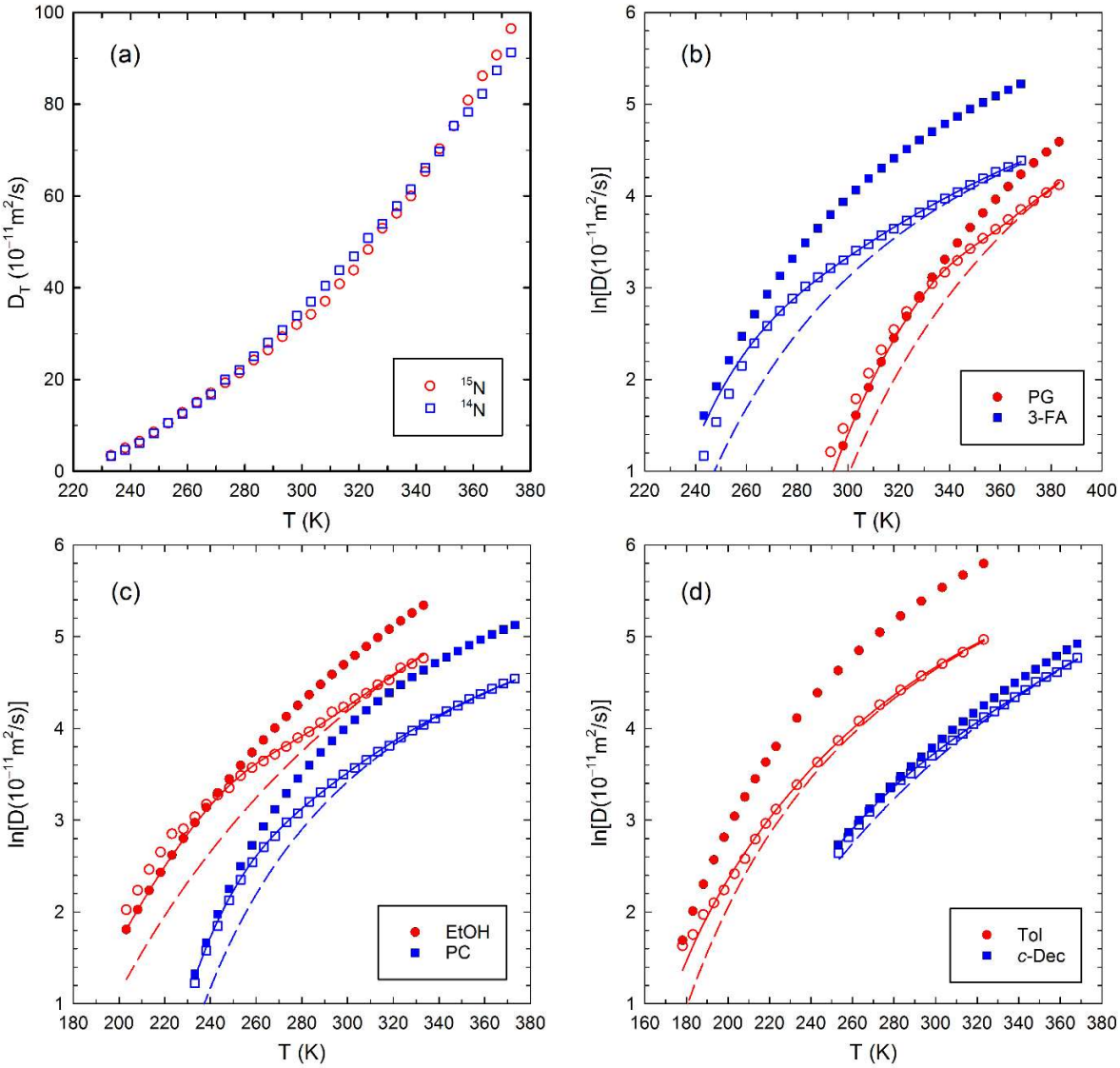

From the SE law for the tracer diffusivity $D_T = k_B T/(6\pi\eta r_T)$, where r_T is the radius of the tracer molecule and η is the viscosity of the solution, the expected tracer to self- diffusivity ratio is:

$$R_d \equiv D_T / D_S = r_S / r_T, \quad (1)$$

where r_S is the radius of the solvent molecule. According to another prediction model for the tracer diffusivity of various solutes in organic solvents and water,[2] this ratio is:

$$R_d = \left(\frac{1 + M_S / M_T}{2}\right)^{1/2} \left(\frac{2}{1 + r_T / r_S}\right)^2, \quad (2)$$

where M_T and M_S are the molecular masses of the tracer and solvent molecules, respectively. Both models predict a constant value of R_d, which depends only on the relative sizes and masses of the tracer and solvent molecules. By using the known masses and calculated radii of the tracer and solvent molecules in our case (Figure S2), the ratios R_d from eqs 1 and 2 were estimated (Table 1). The radii are calculated from the van der Waals volumes obtained by the fast-calculation method,[22] assuming spherical molecular shapes.

In order to relate radical and solvent diffusivities, we collected numerical and graphical self-diffusion data and determined the temperature dependence of self-diffusivity $D_S(T)$ by fitting (Figure S1 and Table S1). Comparing the values of radical diffusivities and the fitted values of self-diffusivities at measured temperatures, we found that the ratio between them R_d varies with temperature in all liquids (Figure 1). At high temperatures, the radical diffusivities are lower than the self-diffusivities implying that

$R_d < 1$ holds, as predicted by eqs 1 and 2. However, the radical and self-diffusivities have similar values at low temperatures, where $R_d \approx 1$ holds. Following the explanation of the weak isotope effect on tracer diffusivity in metallic liquids,[14,17] we propose that the crossover behavior of radical diffusivity upon cooling results from the participation of more and more molecules in the diffusion process, which causes the radical and self- diffusivities to differ less and less.

Table 1. Experimental Values of Melting Temperature T_m, Glass Transition Temperature T_g, and Fragility Index m. Calculated Radical to Self-Diffusivity Ratio R_d by eqs 1 and 2. The Best-Fit Values of Parameters R_H, Δ, and T_{cr} of the Simple Diffusion Model (eq 3). The Best-Fit Values of Arrhenius Crossover Temperatures T_A from Viscosities.

Liquid	T_m (K)	T_g (K)	m	R_d eq 1	R_d eq 2	R_H	Δ (K)	T_{cr} (K)	T_A (K)
PG	211	167	52	0.76	0.63	0.64	18	346	358
EtOH	159	94	55	0.67	0.50	0.58	24	266	199
3-FA	271	173	70	0.82	0.73	0.42	37	269	319
PC	224	160	99	0.80	0.69	0.55	30	267	303
Tol	178	117	103	0.82	0.70	0.43	36	179	236
c-Dec	230	145	149	0.96	0.90	0.84	34	298	337

In order to quantify the crossover phenomenon, we constructed a simple diffusion model where one molecule can diffuse via either a single-molecule process or a collective process in which several molecules participate. Consequently, the self-diffusivity can be expressed as $D_S(T) = D_{S1}(T) + D_{Sc}(T)$, where $D_{S1}(T)$ and $D_{Sc}(T)$ are the single-molecule and collective contributions, respectively, while $D_T(T) = D_{T1}(T) + D_{Tc}(T)$ is an analogous expression for tracer diffusivity. According to eqs 1 and 2, the ratio between the tracer and solvent single-particle diffusivities $R_H = D_{T1}(T)/D_{S1}(T)$ is taken as a temperature-independent constant. Based on the explanation of the weak isotope effect on tracer diffusivity in supercooled metallic liquids,[14,17] we expect that the collective diffusivities of tracer and solvent molecules differ much less than their single-particle diffusivities, and, thus we make a simple assumption $D_{Tc}(T) = D_{Sc}(T)$. By defining the quantity $p_1(T) = D_{S1}(T)/D_S(T)$, the tracer diffusivity can be written as $D_T(T) = D_S(T)R_d(T)$, where the diffusivity ratio is $R_d(T) = R_H p_1(T) + 1 - p_1(T)$. The diffusivity of the solvent molecule in this model depends on the molecule's displacement during the diffusion process and the rate at which this process occurs. If one assumes similar displacements during the single-molecule and collective diffusion processes, the quantity $p_1(T)$ becomes the ratio between the rates of single-molecule and any diffusion processes. Thus, the probabilities that the molecule participates in a given diffusion process as a single entity or part of collective rearrangements are given by p_1 and $p_c = 1 - p_1$, respectively. Supposing a simple two-state behavior of the probabilities, we get $p_1/p_c = \exp\left[-(E_{TS} - TS_{TS})/(k_B T)\right]$. By the general considerations of theory for collective diffusion,[23] the energy difference $E_{TS} > 0$ can be understood as an extra energy cost for the solitary diffusing molecule compared to the molecule that participates in the collective diffusion process. However, the collective

diffusion process demands coherent movements of participating molecules, which gives the extra entropy cost $S_{TS} > 0$ for the molecule that participates in the collective process compared to the solitary diffusing molecule. We can now redefine the two-state parameters by introducing $T_{cr} = E_{TS} / S_{TS}$ as the crossover temperature at which $p_1 = p_c = 1/2$ and $\Delta = 2k_B T_{cr}^2 / E_{TS}$ as half of the temperature width of crossover behavior. Thus, the fitting function for radical diffusivity takes the form:

$$D_T(T) = D_S(T)\left[R_H p_1(T) + 1 - p_1(T)\right];\ p_1(T) = \left[1 + \exp\left(\frac{2T_{cr}}{\Delta}\frac{T_{cr} - T}{T}\right)\right]^{-1} \qquad (3)$$

where $D_S(T)$ is the fitted temperature dependence of self-diffusivity. We listed the best-fit parameters of the fitting function in eq 3 for all liquids (Table 1) and presented the fitted temperature dependences of radical diffusivities (Figure 1). The high-temperature dependences of fitted radical diffusivities $R_H D_S(T)$ are extrapolated to low temperatures to illustrate the crossover effect on radical diffusion (Figure 1), which is indicated by the difference between the experimental data and dashed lines.

By comparing the values of R_d calculated by eqs 1 and 2 with the fitted values of R_H (Table 1), we can see a good agreement for PG, EtOH, and *c*-Dec, while the calculated values are higher than the fitted ones for 3-FA, PC, and Tol. A possible cause of the disagreement for the latter three liquids could be their molecules' non-spherical and disk-like shapes. In order to compare the radical diffusion and Arrhenius crossover phenomena, we estimated the Arrhenius crossover temperatures T_A (Table 1) by fitting the experimental viscosity data available for all liquids (see SI4). We obtained the temperature dependences of viscosities (Figure S6) by using the fitting formula with the parabolic non-Arrhenius term, which was previously applied to analyze metallic liquids' diffusivities.[12] The estimated values of T_A from

the viscosities are checked against the literature values of T_A, which were determined mainly from relaxation time measurements (see SI4). The estimated values of T_A were found to be within or a little higher than the ranges of literature values (Table S3). The estimated temperatures T_A in all studied liquids except EtOH are close to the temperatures $T_{cr} + \Delta$, marking the onset of radical diffusion crossover (Table 1).

The literature values of T_g and kinetic fragility index m for *c*-Dec[24] and other solvents[25] are listed in Table 1, together with the literature values of T_m. Using these values, we presented the relative characteristic temperatures $\theta_{cr} = T_{cr} / T_g$, $\theta_A = T_A / T_g$, and $\theta_m = T_m / T_g$ as a function of m (Figure 2). Error bars denote the crossover regions of radical diffusion, which lie between $\theta_{cr} - \theta_\Delta$ and $\theta_{cr} + \theta_\Delta$, where $\theta_\Delta = \Delta / T_g$ (Figure 2). The fragility index m increases as we go from the hydrogen-bonded liquids PG and EtOH, through the polar liquids 3-FA and PC to the non-polar liquids Tol and *c*-Dec (Table 1). The relative melting temperature θ_m is not correlated with m, and its average value is $\theta_m \approx 1.5$ (Figure 2, red symbols). As we go from the hydrogen-bonded liquids toward 3-FA, PC, and Tol, the relative crossover temperature θ_{cr} decreases toward θ_m, but it increases again for the most fragile *c*-Dec (Figure 2, black symbols). The initial decrease of θ_{cr} agrees with the previous finding[12,13] that some hydrogen-bonded liquids display higher values of θ_A than the other molecular liquids, which generally have $\theta_A \approx 1.4$. However, the increase of θ_{cr} for *c*-Dec is unexpected and will be discussed below. Another unexpected result is that the relative Arrhenius crossover temperature θ_A in our study seems not to be correlated with m (Figure 2, blue symbols). Therefore, we displayed the data for θ_A in molecular liquids from ref 25 (Figure 2, blue crosses). Despite data scattering, we can see that θ_A from this study decreases with m

reaching the value $\theta_A \approx 1.4$ for the highest values of m. This correlation implies that seemingly uncorrelated behavior of θ_A and m in our study results from the lack of experimental points. It seems that our values of θ_A are a little bit higher than expected from the general trend of θ_A against m, which could be the result of our viscosity fitting procedure. However, our values are within the range of data scattering in all studied liquids except in the highly fragile *c*-Dec, where θ_A has an unexpectedly high value (Figure 2).

Figure 2. Relative characteristic temperatures θ versus fragility index m for studied liquids. Symbols mark the crossover temperatures of radical diffusivity $\theta_{cr} = T_{cr} / T_g$ (black), the Arrhenius crossover temperatures $\theta_A = T_A / T_g$ from the viscosity fits (blue), and melting temperatures $\theta_m = T_m / T_g$ (red). Error bars mark the crossover regions of radical diffusivity, which extend from $\theta_{cr} - \theta_\Delta$ to $\theta_{cr} + \theta_\Delta$, where $\theta_\Delta = \Delta / T_g$. Blue crosses denote the data for θ_A taken from ref 25.

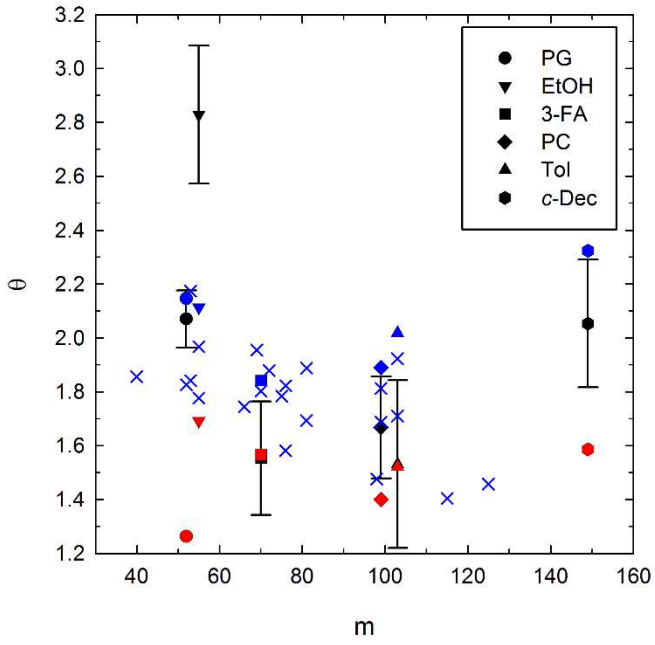

It is interesting to note that *c*-Dec, as one of the most fragile glass former of all, exhibits unexpectedly high values of θ_{cr} and θ_A (Figure 2). The results of neutron scattering measurements and molecular dynamics simulations indicate that molecular neighbor shells in *c*-Dec are much better defined than in a typical molecular glass former cumene with a lower fragility of $m \approx 90$.[24] Moreover, the level of definition of neighbor shells in *c*-Dec is as high as in metallic glass formers. Such unexpected short-range ordering in *c*-Dec could be the reason behind its high values of θ_{cr} and θ_A. Further investigations on this peculiar behavior of *c*-Dec are needed.

Another interesting point is the already mentioned unusual behavior of EtOH, where T_{cr} is significantly higher than T_A (Table 1 and Figure 2). This could relate to the well-known fact that EtOH and other monohydroxy alcohols are inhomogeneous liquids, exhibiting mesoscale structure due to the supramolecular clusters of hydrogen-bonded hydroxyl groups.[26,27] The supramolecular clusters are manifested by the presence of prepeak in addition to the main peak in diffraction spectra of monohydroxy alcohols. The prepeak is clearly visible at room temperature in EtOH,[26] indicating that supramolecular clusters exist above T_{cr} and T_A. Also, the existence of supramolecular clusters in monohydroxy alcohols results in two relaxation processes in structural dynamics: a structural α-relaxation, which is attributed to the dynamics of alkyl chains, and a slower Debye relaxation, which is attributed to dynamics of hydrogen-bonded supramolecular clusters.[26,27] Although Debye relaxation peak strongly contributes to dielectric spectra of monohydroxy alcohols and hinders the α-relaxation peak, the analysis of the true α-relaxation time in EtOH showed that it exhibits the Arrhenius crossover at 200 K,[28] which is equal to T_A from our viscosity analysis (Table 1). Because of the short alkyl chains in EtOH, the radical diffusion is possibly

coupled to α-relaxation governed by alkyl-chain dynamics and Debye relaxation governed by dynamics of hydroxyl groups. The effect of the latter coupling could be a shift of the diffusion crossover temperature T_{cr} to a higher value than T_A. However, further studies of tracer diffusion in various monohydroxy alcohols are needed to clarify this interesting question.

According to molecular dynamics simulations of glass-forming liquids,[15,16] the molecules that cooperatively participate in the collective diffusion process form string-like clusters (strings). The string length n, defined as the number of participating molecules, was found to vary among different strings in very good accordance with the exponential law. This means that the normalized distribution of string lengths has the form $f_n = (1/n_c)(1-1/n_c)^{n-1}$, where n_c is the average string length. The probability that a molecule diffuses as a part of the string with length n is given by $p_n = f_n n/n_c$, which implies that the probability p_1 in eq 3 and n_c are related as $p_1 = n_c^{-2}$. This relationship creates consistency between the observed increase of n_c upon cooling in simulations[15,16] and the decrease of p_1 upon cooling obtained by fitting radical diffusivities to eq 3.

It was recognized that the nearly exponential distribution of string lengths, whose average length grows upon cooling, resembles the distribution of linear polymers formed by equilibrium polymerization upon cooling.[15,16,29] Therefore, several equilibrium polymerization models were used to reproduce the string forming of mobile particles in supercooled liquid.[16,29,30] In the most simple free polymerization model, the polymer chains of associated monomers are characterized by the growth and scission rate constants k_A and k_d, respectively. At the same time, the average chain length is given by $n_c = 1/2 + (1/4 + \phi K_{eq})^{1/2}$, where $K_{eq} = k_A/k_d$ is the equilibrium constant for the polymerization reaction and ϕ is the total concentration of monomers.[30] In the case of weak polymerization $4\phi K_{eq} << 1$,

we get the following relation $p_1 = n_c^{-2} \approx (1 + 2\phi K_{eq})^{-1}$. This relation reproduces p_1 from the fitting function in eq 3 under assumptions that ϕ weakly depends on temperature, and K_{eq} follows the usual Arrhenius law, i.e., $K_{eq} \propto \exp[\Delta h/(k_B T)]$, where Δh is the energy change for chain scission.[16,29,30]

We can conclude that qualitative agreement exists between the assumptions in our simple diffusion model and the behavior of strings in molecular dynamics simulations, which some polymerization models can reproduce. Since polymerization models explain the forming of strings and their behavior only in a phenomenological way without a deeper understanding of underlying mechanisms, we made no attempts to compare our model quantitatively with polymerization models. However, our model offers a link to experimental results for any future diffusion model that will be more physically based. Meanwhile, we expect that our simple diffusion model could be a valuable tool for future studies of tracer diffusion in liquids.

Along with the measurements of the translational diffusivity D_{trans} of tracer and host molecules, the measurements of their rotational diffusivity D_{rot} were found helpful in the studies of crossover phenomenon and heterogeneous dynamics below $T_c \approx 1.2T_g$.[10,11,31] Studies of molecular rotation revealed that the strong SE violation below T_c is accompanied by the so-called translation-rotation decoupling. This decoupling denotes a strong violation of the expected relation for D_{trans}/D_{rot} that combines the SE law for D_{trans} and the Stokes-Einstein-Debye (SED) law for D_{rot}. This result raises the question about the existence of similar decoupling for the crossover detected in our study, which could be answered in future studies by using various techniques to measure the translational and rotational diffusion of host and tracer molecules. In this context, we can mention that the NMR results for host water molecules and the ESR

results for radical tracer molecules indicate translation-rotation decoupling for both molecules close to T_m in the water.[18] Also, we expect that the size-dependent experiments of translational and rotational tracer diffusion, which were applied to study crossover phenomenon and heterogeneous dynamics below T_c ,[10,11,31] could be applied to study the crossover detected in our study.

In summary, we applied the ESR method to obtain the diffusivity of the pDTEMPONE radical at different temperatures in six glass-forming liquids. By comparing the obtained radical diffusivities with the self-diffusivities in all liquids, we checked the theoretical predictions according to which the radical diffusivities should be lower than the self-diffusivities by a constant factor. We found that the predictions are valid only at the highest measured temperatures, while the values of radical diffusivities reach those of self-diffusivities with lowering the temperature. We propose that this crossover behavior of radical diffusivity evidences an increasing number of participating molecules in the diffusion process with temperature lowering. In the theoretical treatment of the crossover phenomenon, we assumed that the diffusivities of both radical and solvent molecules could be separated into contributions from the single-molecule and collective diffusion processes. We defined a simplified diffusion model, where the single-molecule part of radical diffusivity is lower by a constant factor than that of self-diffusivity, while collective parts of the radical and self- diffusivities are the same. In order to quantify the crossover phenomenon, we additionally assumed that the probabilities for the solvent molecule to diffuse in single-molecule or collective processes are interrelated as in the simple two-state system. Thus, we constructed the fitting function for radical diffusivity with temperature parameters T_{cr} and 2Δ , defining the crossover position and its width, respectively. After fitting the experimental radical diffusivities to this function for all liquids, we compared the resulting temperature parameters with the Arrhenius crossover temperatures T_A obtained by fitting experimental viscosity data from the literature. The estimated values of T_A were

found to be close to the onset temperatures of the radical diffusion crossover $T_{cr} + \Delta$ in all studied liquids except ethanol, which suggests that the two crossover phenomena could have the same origin. This origin is very likely the onset of collective behavior of molecular rearrangement upon cooling.

According to the previous studies,[12,13,25] the relative Arrhenius crossover temperature $\theta_A = T_A / T_g$ in glass-forming liquids decreases toward $\theta_m = T_m / T_g$ as their fragility index m increases. Despite a small number of liquids studied here, we found that the relative crossover temperature $\theta_{cr} = T_{cr} / T_g$ generally follows this trend with the exception of *cis*-decalin. To fully establish a correlation between θ_{cr} and m, further studies of θ_{cr} in more glass-forming liquids are needed. We noted that the most fragile *cis*-decalin exhibits relatively high values of θ_{cr} and θ_A, which was tentatively attributed to its unexpectedly high short-range order of molecular neighbor shells.[24] Finally, we showed a general agreement between our simplified treatment of the radical diffusion crossover and the studies of the string-like clusters of diffusing molecules that were detected in molecular dynamics simulations of glass-forming liquids.[15,16,29,30]

Supporting Information

Analysis of self-diffusivity data (SI1), list of molecular properties of materials (SI2), description of ESR method for measuring radical diffusivity (SI3), and estimation of Arrhenius crossover temperatures from viscosities (SI4).

Acknowledgments

This work is supported by the Croatian Science Foundation (Project No. IP-2018-01-3168) and NSF RUI (Grant No. 1856746). The work of doctoral student J. S. has been fully supported by the "Young

researchers' career development project - training of doctoral students" of the Croatian Science Foundation.

References

(1) Suárez-Iglesias, O.; Medina, I.; de los Ángeles Sanz, M.; Pizarro, C.; Bueno, J. L. Self-Diffusion in Molecular Fluids and Noble Gases: Available Data. *J. Chem. Eng. Data* **2015**, *60*, 2757-2817.

(2) Rah, K.; Kwak, S.; Eu, B. C.; Lafleur, M. Relation of Tracer Diffusion Coefficient and Solvent Self-Diffusion Coefficient. *J. Phys. Chem. A* **2002**, *106*, 11841-11845.

(3) Kaintz, A.; Baker, G.; Benesi, A.; Maroncelli, M. Solute Diffusion in Ionic Liquids, NMR Measurements and Comparisons to Conventional Solvents. *J. Phys. Chem. B* **2013**, *117*, 11697-11708.

(4) Molin, Yu. N.; Salikhov, K. M.; Zamaraev, K. I. Spin Exchange Principles and Applications in Chemistry and Biology; Springer−Verlag: Berlin, 1980.

(5) Salikhov, K. M. Contributions of Exchange and Dipole–Dipole Interactions to the Shape of EPR Spectra of Free Radicals in Diluted Solutions. *Appl. Magn. Reson.* **2010**, *38*, 237-256.

(6) Bales, B. L.; Peric, M. EPR Line Shifts and Line Shape Changes Due to Spin Exchange of Nitroxide Free Radicals in Liquids, *J. Phys. Chem. B* **1997**, *101*, 8707−8716.

(7) Merunka, D.; Peric, M. Measuring Radical Diffusion in Viscous Liquids by Electron Paramagnetic Resonance. *J. Mol. Liq.* **2019**, *277*, 886-894.

(8) Liu, Q.; Huang, S.; Suo, Z. Brownian Motion of Molecular Probes in Supercooled Liquids. *Phys. Rev. Lett.* **2015**, *114*, 224301.

(9) Mallamace, F.; Branca, C.; Corsaro, C.; Leone, N.; Spooren, J.; Chen, S.-H.; Stanley, H. E. Transport Properties of Glass-Forming Liquids Suggest That Dynamic Crossover Temperature Is as Important as the Glass Transition Temperature. *P. Natl. Acad. Sci. USA* **2010**, *107*, 22457-22462.

(10) Richert, R.; Samwer, K. Enhanced Diffusivity in Supercooled Liquids. *New J. Phys.* **2007**, *9*, 36.

(11) Sillescu, H. Heterogeneity at the Glass Transition: A Review. *J. Non-Cryst. Solids* **1999**, *243*, 81-108.

(12) Jaiswal, A.; Egami, T.; Kelton, K. F.; Schweizer, K. S.; Zhang, Y. Correlation between Fragility and the Arrhenius Crossover Phenomenon in Metallic, Molecular, and Network Liquids. *Phys. Rev. Lett.* **2016**, *117*, 205701.

(13) Elmatad, Y. S.; Chandler, D.; Garrahan, J. P. Corresponding States of Structural Glass Formers. *J. Phys. Chem. B* **2009**, *113*, 5563-5567.

(14) Schober, H. R. Collectivity of Motion in Undercooled Liquids and Amorphous Solids. *J. Non-Cryst. Solids* **2002**, *307-310*, 40-49.

(15) Donati, C.; Douglas, J. F.; Kob, W.; Plimpton, S. J.; Poole, P. H.; Glotzer, S. C. Stringlike Cooperative Motion in a Supercooled Liquid. *Phys. Rev. Lett.* **1998**, *80*, 2338-2341.

(16) Pazmiño Betancourt, B. A.; Douglas, J. F.; Starr, F. W. String Model for the Dynamics of Glass-Forming Liquids. *J. Chem. Phys.* **2014**, *140*, 204509.

(17) Ehmler, H.; Heesemann, A.; Rätzke, K.; Faupel, F.; Geyer, U. Mass Dependence of Diffusion in a Supercooled Metallic Melt. *Phys. Rev. Lett.* **1998**, *80*, 4919-4922.

(18) Merunka, D.; Peric, M. Continuous Diffusion Model for Concentration Dependence of Nitroxide EPR Parameters in Normal and Supercooled Water. *J. Phys. Chem. B* **2017**, *121*, 5259-5272.

(19) Merunka, D.; Peric, M. An Analysis of Radical Diffusion in Ionic Liquids in Terms of Free Volume Theory. *J. Chem. Phys.* **2020**, *152*, 024502.

(20) Kooser, R. G.; Kirchmann, E.; Matkov, T. Measurements of Spin Concentration in Electron Paramagnetic Resonance Spectroscopy Preparation of Standard Solutions from Optical Absorption. *Concept. Magn. Res.* **1992**, *4*, 145-152.

(21) Salikhov, K. M.; Mambetov, A. Ye.; Bakirov, M. M.; Khairuzhdinov, I. T.; Galeev, R. T.; Zaripov, R. B.; Bales, B. L. Spin Exchange Between Charged Paramagnetic Particles in Dilute Solutions. *Appl. Magn. Reson.* **2014**, *45*, 911-940.

(22) Zhao, Y. H.; Abraham, M. H.; Zissimos, A. M. Fast Calculation of van der Waals Volume as a Sum of Atomic and Bond Contributions and Its Application to Drug Compounds. *J. Org. Chem.* **2003**, *68*, 7368-7373.

(23) Salez, T.; Salez, J.; Dalnoki-Veress, K.; Raphaël, E.; Forrest, J. A. Cooperative Strings and Glassy Interfaces. *P. Natl. Acad. Sci. USA* **2015**, *112*, 8227-8231.

(24) Eibl, S. The Highly Fragile Glass Former Decalin. Ph.D. Dissertation, Paris-Sud University, France, 2009.

(25) Novikov, V. N. Connection Between the Glass Transition Temperature T_g and the Arrhenius Temperature T_A in Supercooled Liquids. *Chem. Phys. Lett.* **2016**, *659*, 133-136.

(26) Böhmer, R.; Gainaru, C.; Richert, R. Structure and Dynamics of Monohydroxy Alcohols - Milestones Towards Their Microscopic Understanding, 100 Years after Debye. *Phys. Rep.* **2014**, *545*, 125-195.

(27) Zhai, Y.; Luo, P.; Nagao, M.; Nakajima, K.; Kikuchi, T.; Kawakita, Y.; Kienzle, P. A.; Y.Z.; Faraone, A. Relevance of Hydrogen Bonded Associates to the Transport Properties and Nanoscale Dynamics of Liquid and Supercooled 2-Propanol. *Phys. Chem. Chem. Phys.* **2021**, *23*, 7220-7232.

(28) Zykova, V. A.; Surovtsev, N. V. Inelastic Light Scattering Study of Hydrogen-Bonded Glass Formers: Glycerol And Ethanol. *J. Non-Cryst. Solids* **2017**, *471*, 429-434.

(29) Douglas, J. F.; Dudowicz, J.; Freed, K. F. Does Equilibrium Polymerization Describe the Dynamic Heterogeneity of Glass-Forming Liquids?. *J. Chem. Phys.* **2006**, *125***,** 144907.

(30) Stukalin, E. B.; Douglas, J. F.; Freed, K. F. Multistep Relaxation in Equilibrium Polymer Solutions: A Minimal Model of Relaxation in "Complex" Fluids. *J. Chem. Phys.* **2008**, *129*, 094901.

(31) Wang, L. M.; Richert, R., Exponential Probe Rotation in Glass-Forming Liquids. *J. Chem. Phys.* **2004**, *120*, 11082-11089.

Supporting Information for

Radical Diffusion Crossover Phenomenon in Glass-Forming Liquids

Jakov Slade[†], Dalibor Merunka,*[,†] and Miroslav Peric[‡]

[†]Division of Physical Chemistry, Ruđer Bošković Institute, Bijenička cesta 54, HR-10000 Zagreb, Croatia

[‡]Department of Physics and Astronomy, California State University, Northridge, Northridge, California 91330, United States

*Corresponding author. E-mail: merunka@irb.hr

SI1. Analysis of self-diffusivity data

Figure S1 shows the self-diffusivity values D_S at different temperatures T for propylene glycol (PG), ethanol (EtOH), 3-fluoroaniline (3-FA), propylene carbonate (PC), toluene (Tol), and *cis*-decalin (*c*-Dec). These data were extracted from the literature, and their temperature ranges are reported in Table S1. Data for PG are reported numerical data[1] and data read from the figure.[2] Data for EtOH are reported numerical data[3] and tabulated data[4] read from the figure.[5] Data for 3-FA are tabulated data[4] read from the figure.[6] Data for PC are reported numerical data[7] and tabulated data[4] in the range 232 to 247 K that were read from the figure.[8] Data for Tol are reported numerical data[9] and tabulated data[4] read from the figures.[10,11] Data for *c*-Dec are tabulated data[4] read from the figure.[10] Temperature dependences of D_S were fitted to the relation:

$$\ln D_S(T) = \ln D_0 - B/(T - T_0), \qquad \text{(S1)}$$

which is the Vogel−Fulcher−Tammann law for $T_0 > 0$ or the Arrhenius law for $T_0 = 0$. The best-fit values are reported in Table S1, and the fits $D_S(T)$ are drawn in Figure S1.

Figure S1. Temperature dependences of self-diffusivities in studied liquids (symbols) and their fits (lines) to the eq S1.

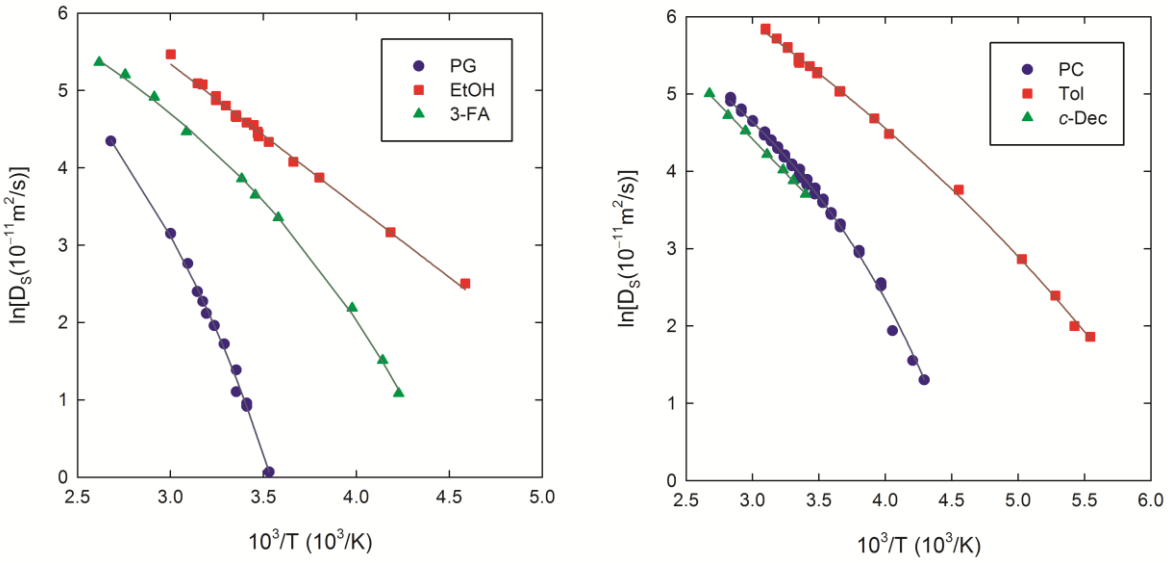

Table S1. Temperature ranges and the best-fit values of the parameters in eq S1 for self-diffusivity data in studied liquids.

Liquid	Temp. range (K)	$\ln D_0 (10^{-11}\mathrm{m}^2/\mathrm{s})$	B (K)	T_0 (K)
PG	283-374	8.85	826	189
EtOH	218-333	10.86	1840	0
3-FA	236-383	7.99	611	147
PC	232-353	7.40	506	150
Tol	180-323	8.82	763	71
c-Dec	294- 374	9.75	1775	0

SI2. Molecular properties of materials

The structures and molar masses of the radical tracer and the glass-forming solvents are shown in Figure S2, where the radical molar mass is the average value of ^{15}N- and ^{14}N-pDTEMPONE. We applied the fast-calculation method[12] to obtain the van der Waals volumes of tracer molecule V_T and solvent molecules V_S. Assuming that the chemicals are spheres, their van der Waals radii were calculated from the formula $r_{T,S} = (3V_{T,S}/4\pi)^{1/3}$, and the calculated values are shown in Figure S2.

Figure S2. Chemical structures, molar masses, and van der Waals radii of pDTEMPONE and glass-forming solvents.

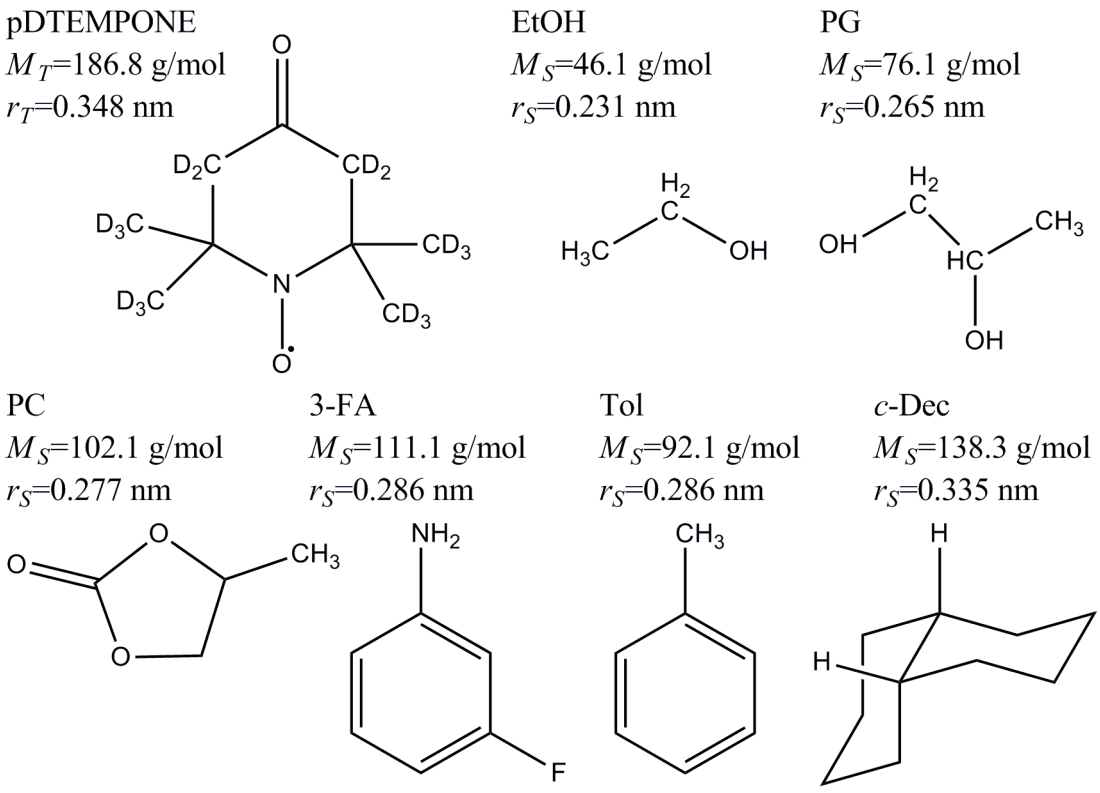

SI3. ESR method for measuring radical diffusivity

Purity of pDTEMPONE radicals

Solutions of Fremy's salt radicals were used as standard solutions to estimate the purity of pDTEMPONE radicals.[13] We prepared five solutions of the ^{15}N-pDTEMPONE, ^{14}N-pDTEMPONE, and Fremy's salt radicals in Na_2CO_3 aqueous solution of 50 mol/m^3. Five nominal concentrations for each radical were determined by weighing, and they were set to be nearly equally spaced. Then, the exact radical concentrations of five Fremy's salt solutions were determined by CARY 50 UV/VIS spectrophotometer, using known molar absorptivity of Fremy's salt in water (2.08 m^2/mol at the wavelength of 545 nm).

Equal volumes of all 15 solutions were drawn into the same type of capillaries, and the ESR spectra for all samples were recorded under the same conditions. Each ESR spectrum was numerically double integrated and fitted to the theoretical spectral function. We found that the values of the double integral and intensity of fitting function linearly depended on the exact concentration of Fremy's salt radicals and the nominal concentration of pDTEMPONE radicals. By calculating the slopes of these linear dependences and comparing them, we found that the ratio between the exact and nominal concentrations is 0.86 for ^{15}N-pDTEMPONE radical and 0.87 for ^{14}N-pDTEMPONE radical.

ESR measurements

We prepared 12 solutions with equally spaced concentrations of ^{15}N- and ^{14}N-pDTEMPONE in each solvent by diluting the stock solutions and determining the nominal concentrations by weighing. For ESR measurements, solutions were drawn into 5-μL capillaries (radius≈150 μm), whose lower end was sealed by Haematocrit sealing compound, and the upper end was left open. ESR spectra were recorded with a Varian E-109 X-band spectrometer upgraded with a Bruker microwave bridge and a

Bruker high-Q cavity. The sample temperature was controlled by a Bruker variable temperature unit and measured with a thermocouple using an Omega temperature indicator. The thermocouple tip was positioned at the top of the active region of the ESR cavity to avoid reducing the cavity quality factor. All samples were measured in steps of 5 K or 10 K in various temperature ranges depending on the properties of each solvent. The ESR spectra were acquired with a sweep time of 20 s, microwave power of 0.5 mW, modulation amplitude of 0.017 mT, and sweep width of 5 mT. The nominal radical concentrations were corrected by factors 0.86 for ^{15}N- and 0.87 for ^{14}N-pDTEMPONE. The radical concentrations were additionally corrected for the temperature dependence of solvents' densities, which was taken from the literature.

Fitting ESR spectra

The experimental ESR spectrum is given by $S(B) = dR(B)/dB$, where $R(B)$ is the absorption ESR signal and B is the applied magnetic field. Since the spin of the nitrogen nucleus I has a value of 1/2 for ^{15}N and 1 for ^{14}N, and the number of hyperfine lines is $2I+1$, the ESR spectra of ^{15}N- and ^{14}N-labeled radicals exhibit two and three hyperfine lines, respectively (Figure S3). The theoretical $R(B)$ for the solutions of ^{15}N- and ^{14}N-labeled radicals, assuming the Heisenberg spin exchange (HSE) and dipole-dipole (DD) spin interactions, was obtained from the modified Bloch equations:[14-17]

$$R(B) = J_0 \,\mathrm{Re}\left[\frac{G(B)}{1-\Lambda G(B)}\right];\; G(B) = \sum_{k=1}^{2I+1} \frac{1}{\Gamma_k + \Lambda + i(B - B_0 - B_k)}, \qquad \text{(S2)}$$

where J_0 is the intensity, Λ is the coherence-transfer rate, Γ_k is the spin dephasing rate of *k*-th line, and B_0 is the central field of the spectrum. The field shifts B_k for ^{15}N-labeled radical are $B_{1,2} = \pm A/2$,

where A is the nitrogen hyperfine splitting, while those for ^{14}N-labeled radical are $B_{1,3} = \pm A + S/3$ and $B_2 = -2S/3$, where S is the second-order hyperfine shift.

Figure S3. ESR spectra (black lines), fits (red lines), and residuals (green lines) for the solutions with 2 and 24 mol/m^3 of ^{15}N- and ^{14}N-pDTEMPONE in PC at 303.15 K.

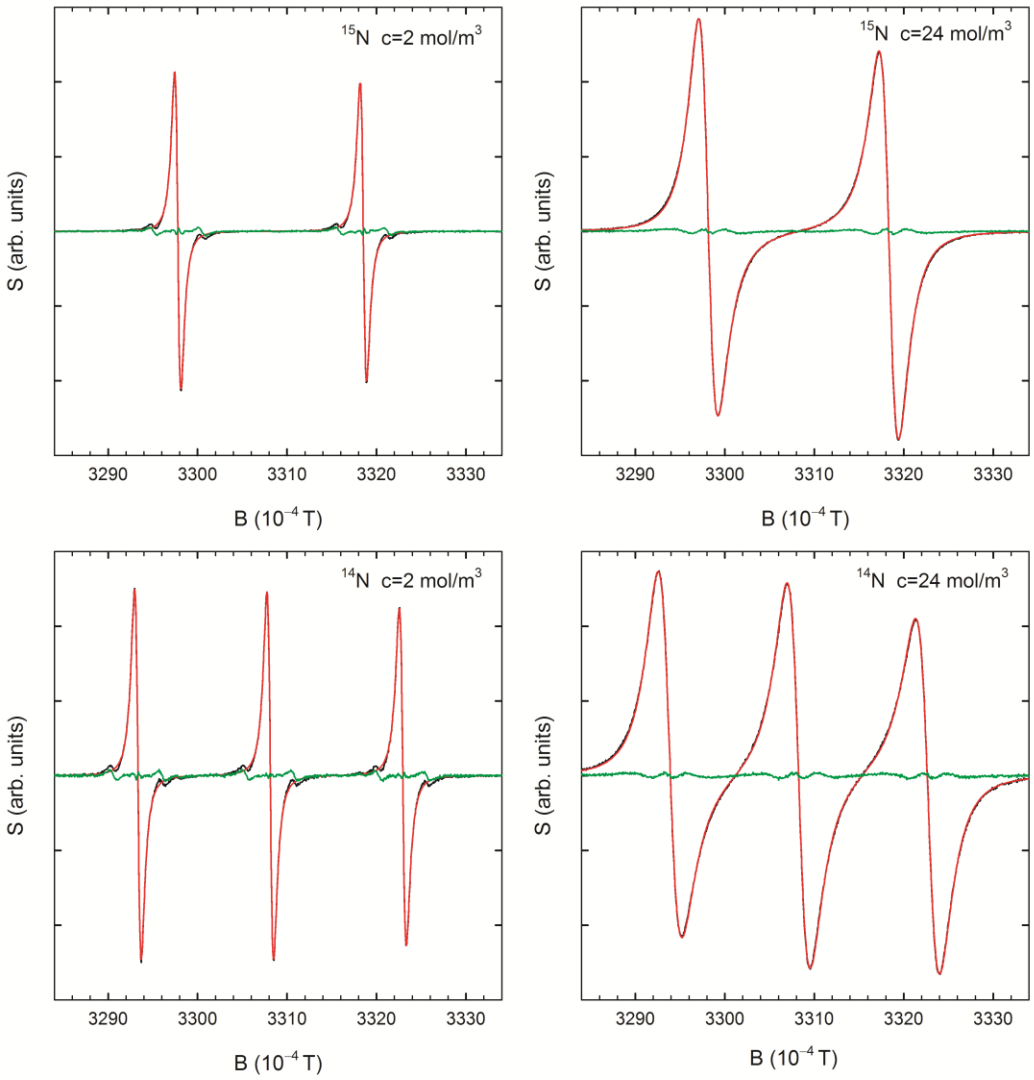

We fitted experimental ESR spectra to the first derivative of $R(B)$ using eq S2. The experimental spectra, fitting curves, and residuals for two concentrations of ^{15}N- and ^{14}N-pDTEMPONE in PC at 303.15 K are shown in Figure S3, while the corresponding best-fit values of ESR parameters are given in Table S2. The increase of Λ with concentration (Table S2) induces dispersion components in the hyperfine lines, which lifts the low field line and pushes down the high field line of spectra for 24 mol/m^3 (Figure S3).

Table S2. The best-fit values of ESR parameters for the solutions with 2 and 24 mol/m^3 of ^{15}N- and ^{14}N-pDTEMPONE in PC at 303.15 K.

Solution	J_0 (arb.u.)	Λ (10^{-4}T)	B_0 (10^{-4}T)	A (10^{-4}T)	Γ_1 (10^{-4}T)	Γ_2 (10^{-4}T)	Γ_3 (10^{-4}T)	S (10^{-4}T)
^{15}N, 2 mol/m^3	115.5	0.084	3308.2	20.746	0.613	0.594	-	-
^{15}N, 24 mol/m^3	1432	1.181	3308.3	20.505	1.897	1.876	-	-
^{14}N, 2 mol/m^3	153.0	0.051	3308.1	14.809	0.661	0.633	0.631	0.010
^{14}N, 24 mol/m^3	1980	0.837	3308.3	14.636	2.321	2.253	2.288	0.019

Obtaining radical diffusivity from the concentration coefficients of ESR parameters

The ESR parameters Γ_k, Λ, and A depend on the radical concentration and diffusivity due to HSE and DD interactions. At low radical concentrations, all parameters are expected to linearly depend on radical concentration with the slopes that depend on radical diffusivity. We analyzed the concentration dependences of Λ (Figure S4), because it gives the best parameter for the calculation of radical diffusivity.[15] The fitted values of Λ at each temperature follow the expected linear dependence

$\Lambda = \Lambda_0 + V_j c$ on the radical concentration c (Figure S4). The linear concentration coefficient V_j, denoted as V_1 for ^{15}N- and V_2 for ^{14}N-pDTEMPONE, was evaluated as the slope of the linear fit (Figure S4). Fits are calculated using the linear regression method with weights being the inverse squares of standard errors from spectral fitting. The temperature dependences of evaluated V_1 and V_2 for PC are shown in Figure S5.

Figure S4. Concentration dependences of the spin coherence-transfer rate Λ for ^{15}N- and ^{14}N-pDTEMPONE in PC at various temperatures (symbols) and their linear fits (lines).

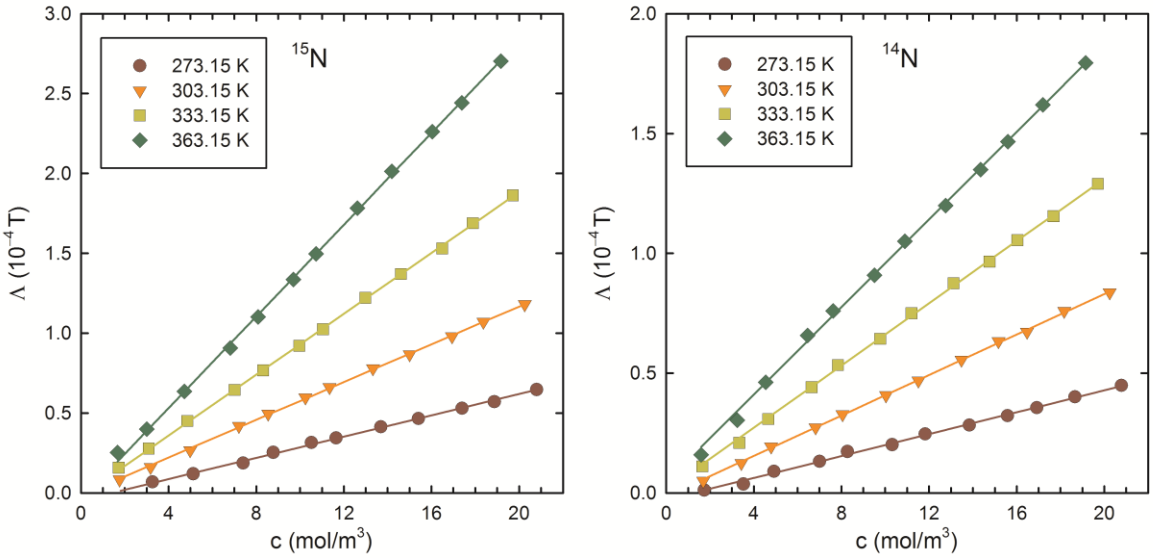

In order to calculate coefficients $V_{1,2}$ as a function of radical diffusivity D_T, we modeled radicals in solution as continuously diffusing hard spheres of radius $\sigma/2$. The relative motion of radicals A and B, characterized by the relative diffusivity $D_r = 2D_T$ and the encounter time $\tau_D = \sigma^2 / D_r$, modulates

the HSE and DD spin interaction. Since the condition $\tau_D\omega_x >> 1$ is satisfied for the X-band frequency and diffusivities of interest, the DD interaction only affects the ESR spectra via modulation of its secular part. The HSE interaction and the secular part of DD interaction have the following forms:

$$H_{HSE} = \hbar J(r)\vec{S}_A\vec{S}_B;\ H_{DD}^{(0)} = \hbar\omega_{DD}(\sigma/r)^3 Y_2^0(\Omega)\left(S_A^+S_B^- + S_A^-S_B^+ - 4S_A^zS_B^z\right), \qquad \text{(S3)}$$

where $\vec{S}_{A,B}$ are spins of radicals, $J(r)$ is the HSE integral, r is the distance between radicals, and Ω denotes the orientation angles between the relative position vector and magnetic field. The DD frequency is $\omega_{DD} = \sqrt{\pi/5}(\hbar\gamma_e^2\mu_0)/(4\pi\sigma^3)$, where γ_e is the electron gyromagnetic ratio.

Figure S5. Experimental values of the concentration coefficients V_1 and V_2 for ^{15}N- and ^{14}N-pDTEMPONE as a function of temperature in PC (symbols) and the theoretical values of these coefficients as a function of radical diffusivity (lines).

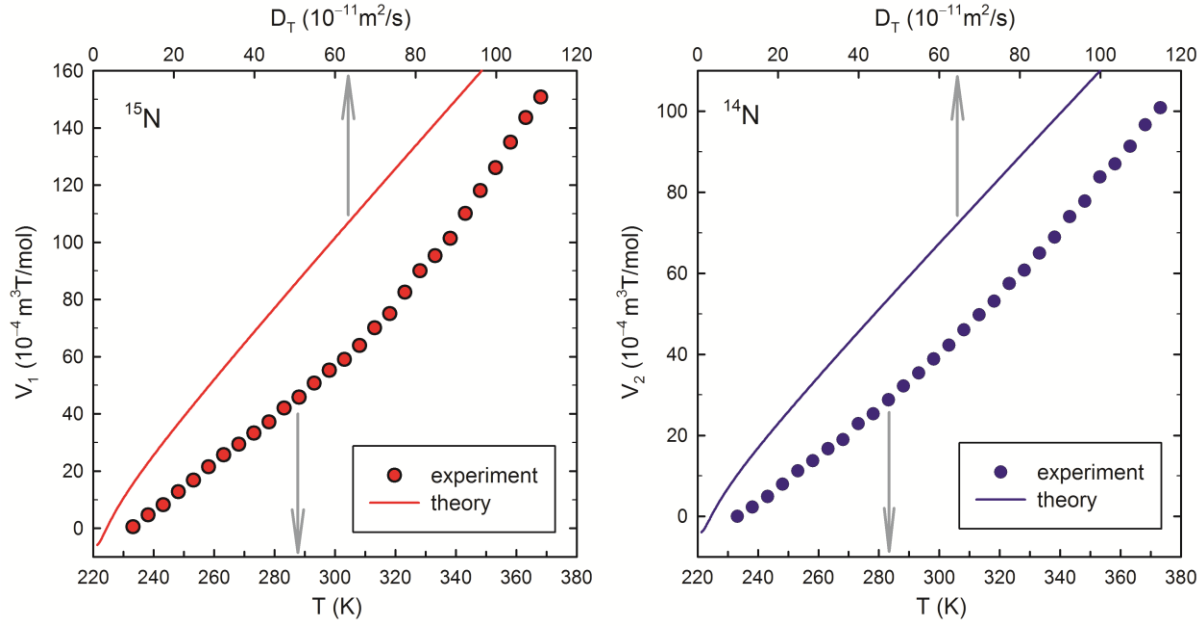

Since $J(r)$ strongly decreases with r, it was approximated by the function having a non-zero value J_0 only in the range of distances $\sigma \le r \le \sigma + \Delta$, where $\Delta << \sigma$ is a small width of the interaction layer. We assumed that J_0 for pDTEMPONE fulfills the strong HSE regime condition $J_0 \tau_C >> 1$, where $\tau_C = \sigma\Delta / D_r$ is the contact time of radicals in the interaction layer. We also assumed that ω_{DD} and the difference in Zeeman frequencies of radicals $\delta = \omega_A - \omega_B$ satisfy $\omega_{DD}\tau_C << 1$ and $|\delta|\tau_C << 1$. Using formalism of the kinetic equations for spin density matrices of radicals,[15,16,18,19] we get:

$$V_1 = \frac{N_A}{2\gamma_e}\left\{k_D \,\mathrm{Re}[p(a)] - \frac{\kappa_{DD}^2}{k_D}\mathrm{Re}[j_\lambda(a)]\right\}, \tag{S4a}$$

$$V_2 = \frac{N_A}{3\gamma_e}\left\{k_D \,\mathrm{Re}\left[\frac{2p(a)+p(2a)}{3}\right] - \frac{\kappa_{DD}^2}{k_D}\mathrm{Re}\left[\frac{2j_\lambda(a)+j_\lambda(2a)}{3}\right]\right\}. \tag{S4b}$$

Here, N_A is the Avogadro constant, $k_D = 4\pi\sigma D_r$ is the rate constant of diffusion encounters, and $\kappa_{DD} = 2\sqrt{\pi}\sigma^3\omega_{DD}$ is the rate constant of the DD interaction. The complex parameter for HSE interaction p and the one for DD interaction j_λ depend on $|\delta|$ between different hyperfine lines, which has possible values a and $2a$, where $a = \gamma_e A$. The complex parameters were calculated by numerically solving the partial differential equations for the functions defining the density matrix of an isolated radical pair.[15] The coefficients $V_{1,2}$ are calculated as a function of D_T (Figure S5) using the van der Waals value $\sigma/2 = 0.35$ nm for the radius of pDTEMPONE (Figure S1) and the experimental values of A in a given liquid (A in PC is set to 2.1 mT for ^{15}N- and 1.5 mT for ^{14}N-pDTEMPONE). By comparing experimental and theoretical values of $V_{1,2}$ at each temperature (Figure S5), we obtained $D_T(T)$ for ^{15}N- and ^{14}N-pDTEMPONE (Figure 1).

SI4. Estimation of the Arrhenius crossover temperatures from viscosities

The obtained literature data for the temperature dependences of viscosity $\eta(T)$ in PG,[20] EtOH,[21] 3-FA,[22] PC,[23] Tol,[24,25] and *c*-Dec[26] are presented in Figure S6. The temperature ranges of these data are reported in Table S3. Viscosity data from refs 21, 22, and 25 are taken from tables in ref 27.

Figure S6. Temperature dependences of viscosities in studied liquids (symbols) and their fits (lines) to the eq S5.

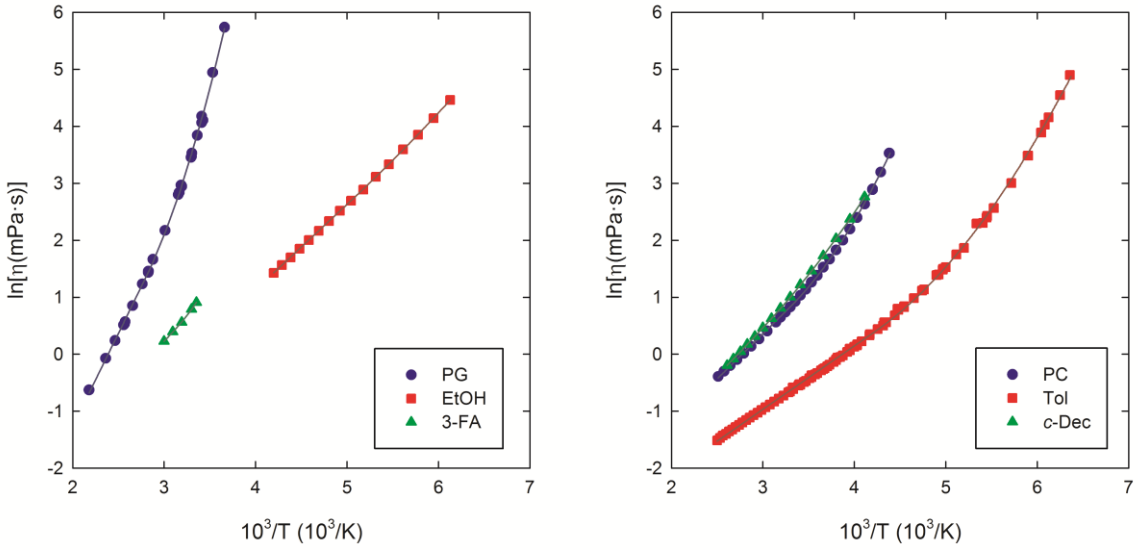

In order to estimate the Arrhenius crossover temperature T_A from viscosity data, we employed a fitting formula that was previously applied on diffusivity data in metallic liquids.[28] We fitted temperature dependences of η using the formula:

$$\ln\eta(T) = \ln\eta_0 + E_\infty/(k_B T) + J^2(1/T - 1/T_A)^2\,\theta(1/T - 1/T_A), \qquad \text{(S5)}$$

where θ is the Heaviside step function. The fitting formula predicts the Arrhenius temperature dependence above T_A, which is defined by the activation energy E_∞ and pre-exponential factor η_0. It also predicts the super-Arrhenius behavior below T_A, which is governed by the parabolic term defined by the parameter J. The obtained best-fit values of all parameters are presented in Table S3, and the fitted $\eta(T)$ are plotted in Figure S6. We found the values of T_A in the literature[29-37] for all liquids except *c*-Dec (Table S3). The reported values were obtained mainly by analyzing relaxation time data. We can see that our values of T_A are within the range of reported values (EtOH, Tol) or a little bit higher than them (PG, 3-FA, PC).

Table S3. Temperature ranges of analyzed viscosity data in studied liquids, the best-fit values of the parameters in eq S5, and the literature values of Arrhenius crossover temperatures with references.

Liquid	Temp. range (K)	$\ln\eta_0$(mPa·s)	E_∞/k_B (K)	J (K)	T_A (K)	T_A(Lit.) (K)
PG	273-459	−7.78	3258	1438	358	305,[29] 308,[29] 321[30]
EtOH	163-238	−4.86	1498	344	199	165,[31] 186,[32]200,[33] 213,[29] 219[29]
3-FA	298-333	−5.05	1757	1189	319	225,[30] 312[34]
PC	228-398	−4.40	1585	905	303	235,[35] 264,[36]269,[37] 270,[34] 286,[32] 287,[29] 290[31]
Tol	157-400	−4.31	1115	677	236	193,[36] 200,[34] 220,[37] 225,[29] 255[29]
c-Dec	243-383	−4.62	1692	561	337	-

References

(1) D'Agostino, C.; Ryabenkova, Y.; Miedziak, P. J.; Taylor, S. H.; Hutchings, G. J.; Gladden, L. F.; Mantle, M. D. *Catal. Sci. Technol.* **2014**, *4*, 1313; Ferreira, E. S. C.; Voroshylova, I. V.; Koverga, V. A.; Pereira, C. M.; Cordeiro, M. N. D. S. *J. Phys. Chem. B* **2017**, *121*, 10906; Rodnikova, M. N. Idiyatullin, Z. Sh.; Solonina, I. A. *Russ. J. Phys. Chem. A* **2014**, *88*, 1442.

(2) Korpała, A. Ph.D. Dissertation, Jagiellonian University, Poland, 2016.

(3) Karger, N.; Vardag, T.; Lüdemann, H.-D. *J. Chem. Phys.* **1990**, *93*, 3437; Holz, M.; Mao, X.; Seiferling, D.; Sacco, A. *J. Chem. Phys.* **1996**, *104*, 669; Tofts, P. S.; Lloyd, D.; Clark, C. A.; Barker, G. J.; Parker, G. J. M.; McConville, P.; Baldock, C.; Pope, J. M. *Magn. Reson. Med.* **2000**, *43*, 368; Price, W. S.; Ide, H.; Arata, Y. *J. Phys. Chem. A* **2003**, *107*, 4784.

(4) Suárez-Iglesias, O.; Medina, I.; de los Ángeles Sanz, M.; Pizarro, C.; Bueno J. L. *J. Chem. Eng. Data* **2015**, *60*, 2757.

(5) Meckl, S.; Zeidler, M. D. *Mol. Phys.* **1988**, *63*, 85.

(6) Kircher, O.; Böhmer, R.; Alba-Simionesco, C. *J. Mol. Struct.* **1999**, *479*, 195.

(7) Harris, K. R.; Kanakubo, M. *J. Chem. Eng. Data*, **2016**, *61*, 2399; Rodnikova, M. N.; Samigullin, F. M.; Solonina, I. A.; Sirotkin, D. A. *J. Struct. Chem.* **2014**, *55*, 256.

(8) Qi, F.; Schug, K. U.; Dupont, S.; Döß, A.; Böhmer, R.; Sillescu, H.; Kolshorn, H.; Zimmermann, H. *J. Chem. Phys.* **2000**, *112*, 9455.

(9) Harris, K. R.; Alexander, J. J.; Goscinska, T.; Malhotra, R.; Woolf L. A.; Dymond, J. H. *J. Mol. Phys.* **1993**, *78*, 235.

(10) Fisher, J.; Weiss, A. *Ber. Bunsenges. Phys. Chem.* **1986**, *90*, 896.

(11) Hinze, G.; Sillescu, H. *J. Chem. Phys.* **1996**, *104*, 314.

(12) Zhao, Y. H.; Abraham, M. H.; Zissimos, A. M. *J. Org. Chem.* **2003**, *68*, 7368.

(13) Kooser, R. G.; Kirchmann, E.; Matkov, T. *Concept. Magn. Res.* **1992**, *4*, 145.

(14) Salikhov, K. M. *Appl. Magn. Reson.* **2010**, *38*, 237.

(15) Merunka, D.; Peric, M. *J. Mol. Liq.* **2019**, *277*, 886.

(16) Merunka, D.; Peric, M. *J. Phys. Chem. B* **2017**, *121*, 5259.

(17) Merunka, D.; Peric, M. **2020**, *152*, 024502.

(18) Molin, Yu. N.; Salikhov, K. M.; Zamaraev, K. I. *Spin Exchange Principles and Applications in Chemistry and Biology*; Springer−Verlag: Berlin, 1980.

(19) Salikhov, K. M.; Mambetov, A. Ye.; Bakirov, M. M.; Khairuzhdinov, I. T.; Galeev, R. T.; Zaripov, R. B.; Bales, B. L. *Appl. Magn. Reson.* **2014**, *45*, 911.

(20) Sagdeev, D. I.; Fomina, M. G.; Abdulagatov, I. M. *Fluid Phase Equilib.* **2017**, *450*, 99; Gary, J. H.; Crichton, J. S.; Feild, R. *Ind. Eng. Chem. Chem. Eng. Data Series* **1958**, *3*, 111; Sun, T.; Teja, A. S. *J. Chem. Eng. Data* **2004**, *49*, 1311.

(21) Golubev, I. F.; Pogikhonova, T. M. *Tr. Gos. Nauchn. Issledov. Proekt. Inst. Azotn. Prom.* **1971**, *8*, 67.

(22) Swarts, F. *J. Chim. Phys.* **1931**, *28*, 622.

(23) Barthel, J.; Neueder, R.; Roch, H. *J. Chem. Eng. Data* **2000**, *45*, 1007; Barthel, J.; Gores, H.-J.; Carlier, P.; Feuerlein, F.; Utz, M. *Ber. Bunsenges. Phys. Chem.* **1983**, *87*, 436.

(24) Santos, F. J. V.; Nieto de Castro, C. A.; Dymond, J. H.; Dalaouti, N. K.; Assael, M. J.; Nagashima, A. *J. Phys. Chem. Ref. Data* **2006**, *35*, 1; Barlow, A. J.; Lamb, J.; Matheson, A. J. *Proc. R. Soc. Lond. A* **1966**, *292*, 322.

(25) Rabe, D. Ph.D. Dissertation, TU Berlin, Germany, 1981; Fieggen, W.; Gerding, H. *Recl. Trav. Chim. Pays-Bas* **1970**, *89*, 236.

(26) Seyer, W. F.; Leslie, J. D. *J. Am. Chem. Soc.* **1942**, *64*, 1912.

(27) Wohlfarth, Ch.; Wohlfahrt, B. *Landolt-Börnstein - Group IV Physical Chemistry, Volume 18B: Viscosity of Pure Organic Liquids and Binary Liquid Mixtures - Pure Organic Liquids*, Springer-Verlag: Berlin, Heidelberg, 2002.

(28) Jaiswal, A.; Egami, T.; Kelton, K. F.; Schweizer, K. S.; Zhang, Y. *Phys. Rev. Lett.* **2016**, *117*, 205701.

(29) Popova, V. A.; Surovtsev, N. V. *J. Chem. Phys.* **2011**, *135*, 134510.

(30) Elmatad, Y. S.; Chandler, D.; Garrahan, J. P. *J. Phys. Chem. B* **2009**, *113*, 5563.

(31) Stickel, F., Fischer, E. W.; Richert, R. *J. Chem. Phys.* **1996**, *104*, 2043.

(32) Ikeda, M.; Aniya, M. *J. Therm. Anal. Calorim.* **2018**, *132*, 835.

(33) Zykova, V. A.; Surovtsev, N. V. *J. Non-Cryst. Solids* **2017**, *471*, 429.

(34) Novikov, V. N. *Chem. Phys. Lett.* **2016**, *659*, 133.

(35) Kivelson, D.; Tarjus, G.; Zhao, X.; Kivelson, S. A. *Phys. Rev. E* **1996**, *53*, 751.

(36) Pazmiño Betancourt, B. A.; Douglas, J. F.; Starr, F. W.; Glotzer, S. C. *J. Chem. Phys.* **2014**, *140*, 204509.

(37) Caruthers, J. M.; Medvedev, G. A. *Phys. Rev. Mater.* **2018**, *2*, 055604.